ADVANCED MATERIALS
www.advmat.de

Integrating Light Diffusion and Conversion Layers for Highly Efficient Multicolored Fiber-Dye-Sensitized Solar Cells

Jiatian Song, Yu Gu, Zhengmeng Lin, Jiuzhou Liu, Xinyue Kang, Xiaocheng Gong, Peiyu Liu, Yiqing Yang, Hongyu Jiang, Jiaqi Wang, Siwei Cao, Zhengfeng Zhu, and Huisheng Peng**

Fiber solar cells as promising wearable power supplies have attracted increasing attentions recently, while further breakthrough on their power conversion efficiency (PCE) and realization of multicolored appearances remain urgent needs particularly in real-world applications. Here, a fiber-dye-sensitized solar cell (FDSSC) integrated with a light diffusion layer composed of alumina/polyurethane film on the outmost encapsulating tube and a light conversion layer made from phosphors/TiO_2/poly(vinylidene fluoride-*co*-hexafluoropropylene) film on the inner counter electrode is designed. The incident light is diffused to more surfaces of fiber electrodes, then converted on counter electrode and reflected to neighboring photoanode, so the FDSSC efficiently takes advantage of the fiber shape for remarkably enhanced light harvesting, producing a record PCE of 13.11%. These efficient FDSSCs also realize color-tunable appearances, improving their designability and compatibility with textiles. They are further integrated with fiber batteries as power systems, providing a power solution for wearables and emerging smart textiles.

1. Introduction

In recent years, the prosperities of wearable technologies in many important fields like information interaction, health monitoring, and personal health management have boosted the developments of the Internet of Things, promoting intelligent life for humans in the future.[1–3] Both current wearables and emerging smart electronic textiles, which are integrating more functions and consuming more electrical power, are raising pressing needs for wearable power supplies, with a special focus on effectivities and sustainability.[4–6] To this end, flexible and lightweight fiber solar cells that can be woven into textiles, as efficient real-time energy harvesting devices in the light environment, have been widely explored to address this challenging power issue.[7–12] However, despite extensive efforts in terms of material innovations in fiber electrodes,[13,14] device structural designs,[15,16] and optimizations of interfaces between active layers,[17] the natural difficulties in fabricating high-quality films and establishing stable interfaces on curved fibers have resulted in fiber solar cells exhibiting comparatively low power conversion efficiencies (PCEs). This limitation has restricted their further development and practical applications in wearables.[12,18–20] An alternative strategy to overcome this bottleneck problem is maximizing the utilization of active layers encompassing fiber electrodes to enhance light harvesting. Fiber solar cells, owing to their unique shape, have the advantage of absorbing incident light from all directions (360°), in contrast to their planar counterparts. Despite the urgent demand, the nondiffusing linear propagation of incident light makes it highly challenging for realization. Therefore, the efficient control of optical field distribution around fiber solar cell is crucial, even though a feasible method is currently unavailable.

Moreover, fiber solar cells woven into textiles are always exposed to the surroundings for light harvesting, and thus the compatibilities of their colors and appearances with textiles also need to be considered for real wearable applications. However, the colored appearances of the outmost encapsulation usually show severe conflict with the requirement for its high transmittance, and the direct use of colorful semitransparent encapsulating tubes would bring about serious performance degradations of fiber solar cells. That is, further realizing highly efficient multicolored fiber solar cells is doubly difficult, but extremely urgent in practical applications.

In this work, we have designed a fiber-dye-sensitized solar cell (FDSSC) integrated with a light diffusion layer on the outmost encapsulating tube and a light conversion layer on the inner counter electrode (**Figure 1a**). The light diffusion layer composed

J. Song, Z. Lin, J. Liu, X. Kang, X. Gong, P. Liu, Y. Yang, H. Jiang, J. Wang, S. Cao, Z. Zhu, H. Peng
State Key Laboratory of Molecular Engineering of Polymers, Department of Macromolecular Science, and Institute of Fiber Materials and Devices
Fudan University
Shanghai 200438, China
E-mail: zhuzf@fudan.edu.cn; penghs@fudan.edu.cn
Y. Gu
Key Laboratory of Advanced Display Materials and Devices
Ministry of Industry and Information Technology
Institute of Optoelectronics & Nanomaterials
College of Material Science and Engineering
Nanjing University of Science and Technology
Nanjing 210094, China

The ORCID identification number(s) for the author(s) of this article can be found under https://doi.org/10.1002/adma.202312590

DOI: 10.1002/adma.202312590

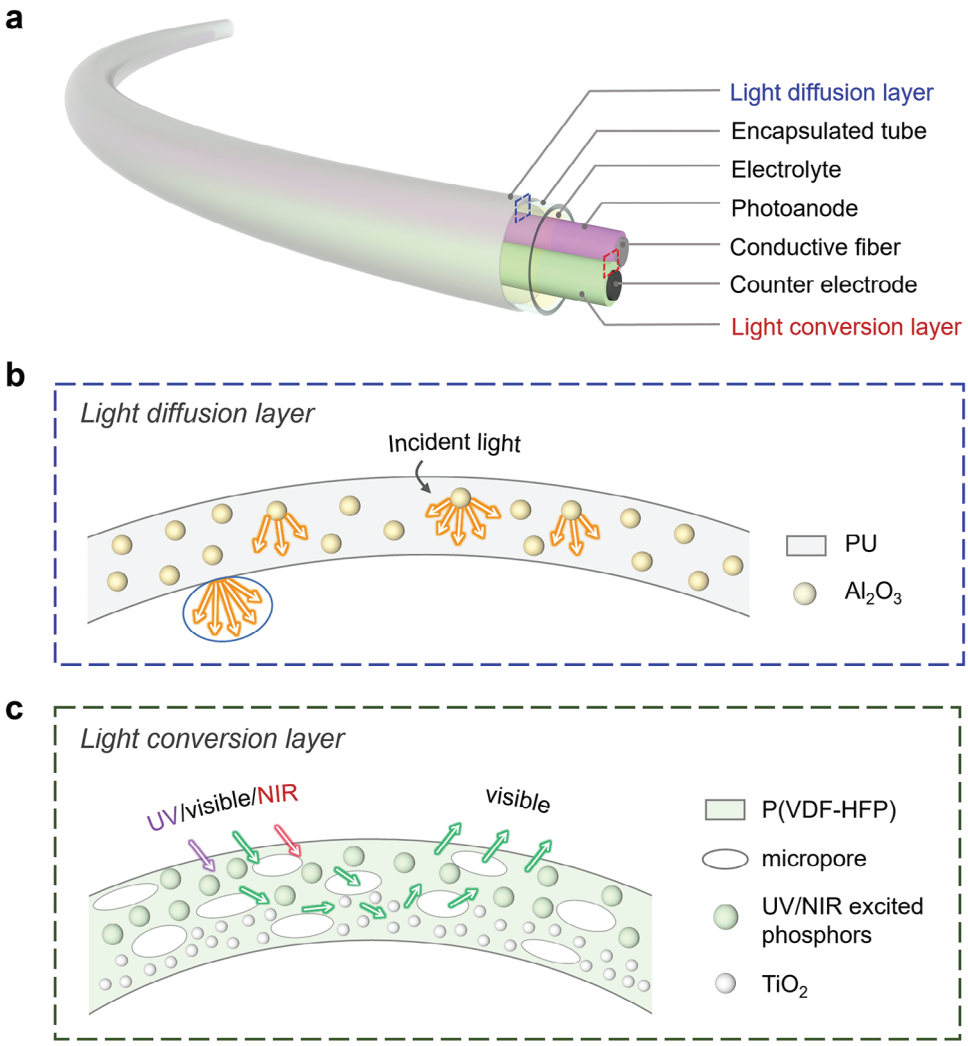

Figure 1. Schematic diagram of FDSSC integrated with light diffusion and conversion layers. a) Diagram illustrating the device structure of FDSSC with a light diffusion layer on the outmost encapsulating tube and a light conversion layer on the inner counter electrode. b) Sketch map of the structure of light diffusion layer composed of PU matrix dispersed with Al_2O_3 particles. The incident light would experience strong refractions and scatterings, and then diffused to more surfaces of fiber electrodes. c) Diagram showing the structure of light conversion layer made from the incorporation of UV/NIR phosphors and TiO_2 nanoparticles into P(VDF-HFP) film. UV and NIR parts of incident light reaching the light conversion layer would be converted by the phosphors to visible wavelengths, and then the whole light was strongly refracted and scattered by the incorporated particles, and eventually propagated out of the layer with reflection.

of a polyurethane (PU) film dispersed with alumina (Al_2O_3) particles showed a dual characteristic of high average transmittance at 88% and high average haze at 82% within the wavelength range of 300–1200 nm, which also gave the FDSSC a white appearance. The light conversion layer, formed by a poly(vinylidene fluoride-*co*-hexafluoropropylene) [P(VDF-HFP)] film containing ultraviolet (UV)/near-infrared (NIR) excited phosphors and TiO_2 nanoparticles, was able to convert UV and NIR light into wavelengths that overlap with the absorption spectrum of active N719 dye. Impressively, this layer exhibited a high reflectivity of over 90%. Therefore, the incident light across Al_2O_3/PU film was diffused to a larger surface area of the fiber electrode. Meanwhile, light reaching the phosphor/P(VDF-HFP) layer would be converted and subsequently be reflected to the neighboring photoanode (Figure 1b,c). The resultant FDSSCs made optimal use of their fiber shape to harvest more incident light, resulting in a remarkable increase of photocurrent and producing a record PCE of 13.11%. These FDSSCs can also realize multicolored appearances by introducing few pigments in light diffusion layer and maintain high PCEs, greatly improving their designability and compatibility in real applications. They were further integrated with fiber batteries into textiles as next-generation power systems.

2. Results and Discussion

Figure 2a schematically illustrates the fabrication process of FDSSCs with light diffusion and conversion layers. Briefly, a high catalytic conducting fiber was coated with a slurry containing the as-prepared phosphor/P(VDF-HFP) slurry with dip-coating.

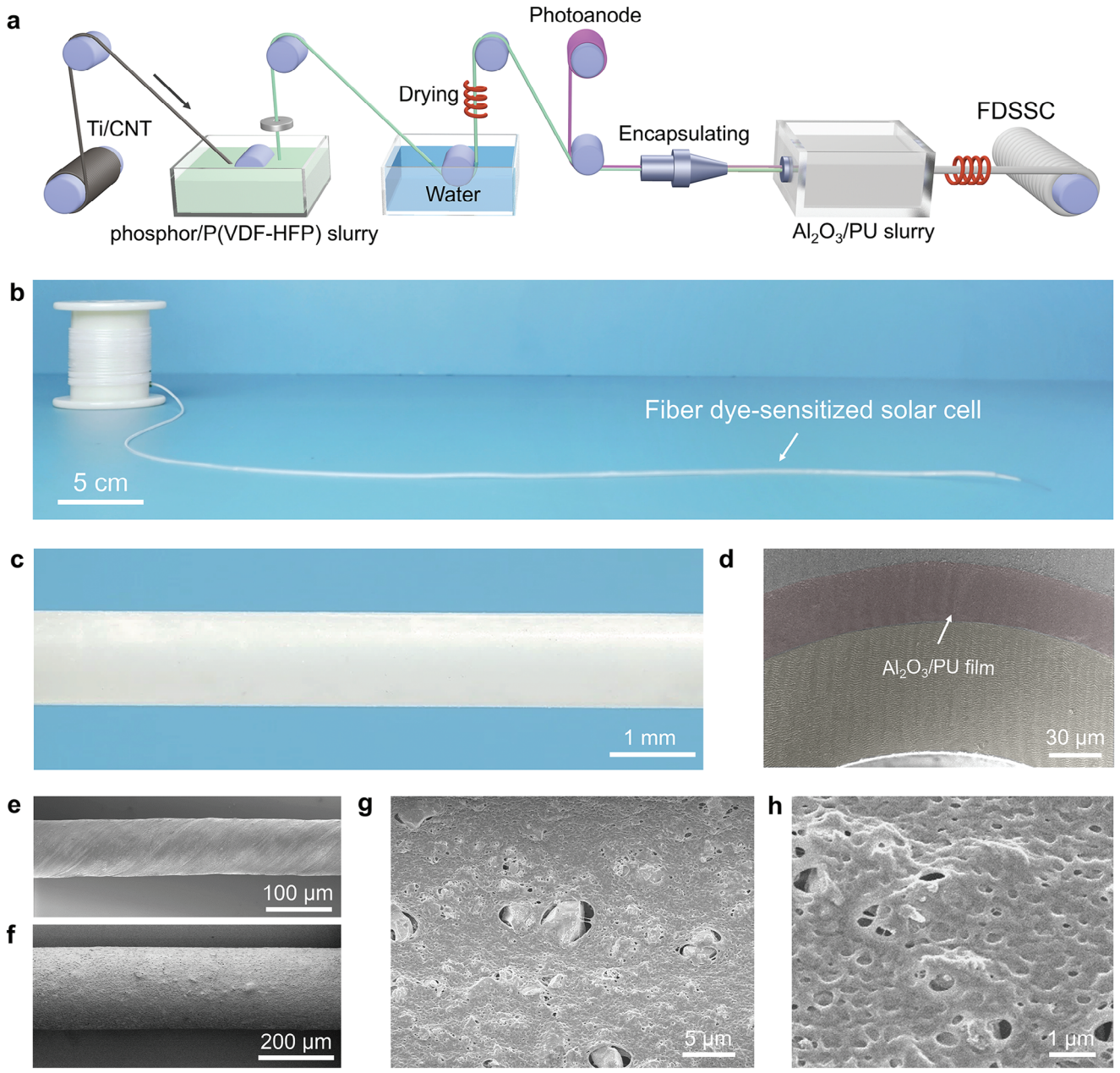

Figure 2. Preparation and structure of the designed FDSSC with light diffusion and conversion layers. a) Diagram illustrating the preparation flow of the FDSSC. After the phosphor/P(VDF-HFP) slurry was dip-coated on a conducting fiber with high catalytic property, it underwent a nonsolvent exchange process in water and the subsequent drying to achieve a fiber counter electrode. The counter electrode was then twisted with a fiber photoanode encapsulated into a transparent tube, which was further coated with an Al_2O_3/PU slurry and dried, followed by injection of an electrolyte to produce the FDSSC. b) Photograph of the fabricated FDSSC. c) Amplified photograph of the FDSSC, in which the encapsulating tube covered with Al_2O_3/PU film as light diffusion layer, displaying a uniform and smooth white appearance. d) Cross-sectional scanning electron microscopy (SEM) image of the encapsulating tube covered with Al_2O_3/PU film, showing a compact interface. e) SEM image of inner conducting fiber in the counter electrode consisting of aligned CNT sheet closely attached to a Ti wire. f) SEM image of phosphor/P(VDF-HFP) film on Ti/CNT fiber. g,h) Magnified SEM images of phosphor/P(VDF-HFP) film with a porous structure, where phosphors were embedded in P(VDF-HFP), at low and high magnifications, respectively.

Subsequently, the fiber underwent a nonsolvent exchange process in water,[21,22] followed by air drying to yield a hybrid fiber counter electrode featuring a porous light conversion layer. The above counter electrode, along with a fiber photoanode made from aligned TiO_2 nanotubes synthesized on a Ti wire by anodization (Figure S1, Supporting Information), was encapsulated into a transparent tube. This tube was dip-coated with an Al_2O_3/PU slurry and went through a subsequent drying to create a light diffusion layer. After being injected with the electrolyte, the final FDSSC (Figure 2b and Figure S2 (Supporting Information)) exhibited a uniform and smooth white appearance, effectively shading the inner fiber electrodes and electrolyte. This outcome

highlighted the remarkable light diffusion effect of the Al_2O_3/PU film tightly attached to the encapsulating tube (Figure 2c,d).

The conducting fiber used in the hybrid fiber counter electrode featured a core–sheath structure. This structure was created by wrapping an aligned carbon nanotube (CNT) sheet synthesized through floating catalyst chemical vapor deposition on a Ti wire (Figure 2e and Figure S3 (Supporting Information)). The resulting design achieved a combination of high conductivity and high catalytic property.[23,24] For further construction of a robust and uniform light conversion layer on Ti/CNT fiber, we introduced P(VDF-HFP) into the phosphor slurry to prepare an organic–inorganic composite film,[25] as pure phosphor film exhibited extremely poor mechanical properties (Figure S4, Supporting Information). Suitable viscosity of phosphor/P(VDF-HFP) slurry is critical for preparing high-quality film on fibers with dip-coating method, as low-viscosity slurry cannot overcome the surface tension, resulting in bead-like aggregations (Figure S5, Supporting Information). While increasing the polymer content in the phosphor/P(VDF-HFP) slurry enhanced its viscosity, and this improvement also had a drawback. High viscosity may lead to excessive adherence of slurry to fiber surfaces, causing irregular aggregations. Hence, we designed pinhole scrapers tailored to the desired fiber diameters to eliminate the excess slurry (Figure S6, Supporting Information), successfully producing uniform phosphor/P(VDF-HFP) layers with precisely controlled thicknesses on fibers (Figure 2f). The obtained film also had high flexibility and mechanical strength, showing no cracks even under bending at a curvature radius of 1.6 mm (Figure S7, Supporting Information).

After the phosphor/P(VDF-HFP) slurry was dip-coated on fiber, a nonsolvent-induced phase separation process would produce great amounts of pores with sizes of hundreds of nanometers in light conversion layer, establishing a stable and continuous channel for the rapid diffusion of ions in the electrolyte (Figure 2g,h and Figures S8 and S9 (Supporting Information)). Although the porous structure inherently had led to a high film reflectance, we also incorporated TiO_2 nanoparticles with sizes of 200–400 nm into the bottom of porous P(VDF-HFP) matrix to further enhance the reflection of light conversion layer (Figures S10 and S11, Supporting Information), as the high refractive index contrast between TiO_2 and P(VDF-HFP) can cause stronger light scatterings.[26–28]

We investigated optical properties of both light diffusion and conversion layers, as they played great roles in the photovoltaic performance of FDSSCs. In light diffusion layer, we used highly transparent PU with high wear resistance, flexibility, and stability as polymer matrix,[29–31] incorporated with Al_2O_3 as light diffusion particle, as they have a proper difference in refractive index. Too small difference in refractive index would not effectively scatter the incident light for diffusion, while too large difference would easily cause backscattering.[32–34] Appropriate sizes and contents of Al_2O_3 particles are critical to light diffusion layer for high light transmittance and high haze.[34,35] We used Al_2O_3 particles with sizes of 1–3 µm because of their strong forward Mie scatterings at UV–visible–NIR wavelengths for efficient light diffusion,[36–38] and a high haze across the wavelength range of 300–1200 nm was achieved (**Figure 3a**). The increase in Al_2O_3 contents effectively improved the haze of Al_2O_3/PU film, and then more incident light was diffused to wider surface areas of fiber electrodes, generating more photocurrents for higher photovoltaic performance of FDSSC (Figure S12, Supporting Information). However, excessive Al_2O_3 particles may severely decrease the film transmittance, leading to the deterioration of photovoltaic performance. The optimal content of Al_2O_3 in PU film was ≈10 wt%, resulting in both high average transmittance of 88% and average haze of 82%. Compared to the traditional FDSSC without light diffusion, which showed a PCE of 9.84% with short-circuit current (J_{SC}), open-circuit voltage (V_{OC}), and fill factor (FF) of 17.730 mA cm^{-2}, 0.735 V, and 0.755, respectively, the FDSSC with the optimal light diffusion layer achieved a higher J_{SC} of 19.215 mA cm^{-2}, producing a PCE of 10.71% (Table S2, Supporting Information). Furthermore, the light diffusion layer showed both high flexibility and mechanical strength (Figure S13, Supporting Information), fully meeting the demands for weaving applications.

In light conversion layer, we added UV excited phosphor ($BaMgAl_{10}O_{17}$:Mn^{2+}, Eu^{2+}) and NIR excited phosphor ($NaYF_4$:Yb^{3+}, Er^{3+}), which were rare earth phosphors with high luminescent quantum efficiency and chemical stability (Figures S14–S17, Supporting Information).[39–41] They can efficiently convert UV light at wavelengths of 300–420 nm and NIR light at wavelengths of 900–1200 nm into visible light (Figure 3b,c and Figure S18 (Supporting Information)). Meanwhile, this layer also exhibited high reflectivity of average value over 90% at wavelengths of 350–800 nm, which precisely aligned with the absorption spectrum of N719 dye (Figure 3d). Therefore, the incident light reaching the light conversion layer would be converted, and then reflected to the neighboring photoanode loaded with N719 dye, realizing more light absorption and also extending the utilization of solar spectrum. By optimizing the concentration of UV/NIR excited phosphors and thickness of the corresponding layer, the highest luminescence intensity was achieved with incorporation of 30 wt% UV excited phosphors and 35 wt% NIR excited phosphors into 50 µm P(VDF-HFP) film (Figures S19 and S20, Supporting Information). Fewer phosphors would not be sufficient for high emission intensity, while excessive phosphor contents in films would cause serious fluorescence quenching.[42–44]

We further simulated the optical field distribution in the FDSSC to illustrate mechanism of the optical enhancement (Figure 3e–g). The optical simulation was conducted with a slight revision of the standard Monte Carlo simulation for photon transport,[45] and the simulation details can be observed in the experimental procedure. Figure 3e gives the simulated structures and the layers with different functions assigned to different boundary conditions in the simulation. Figure 3f corresponds to the FDSSC without light diffusion or conversion layers, showing a collimated incoming light and perfect photon absorptions on both electrodes. It is obvious that light harvesting by photoanode is very limited for the collimated light, as portion of light is fully absorbed by counter electrode or directly passes through the device, leading to a waste of energy from incident light. Figure 3g includes an encapsulating shell that diffuses the incoming light and a counter electrode that reflects the light diffusively. An efficient control of optical field was achieved with light being concentrated in the vicinity of both electrodes, and no light leakage had been observed. The optical filed around photoanode is obviously enhanced, so a more efficient harvest of light is anticipated.

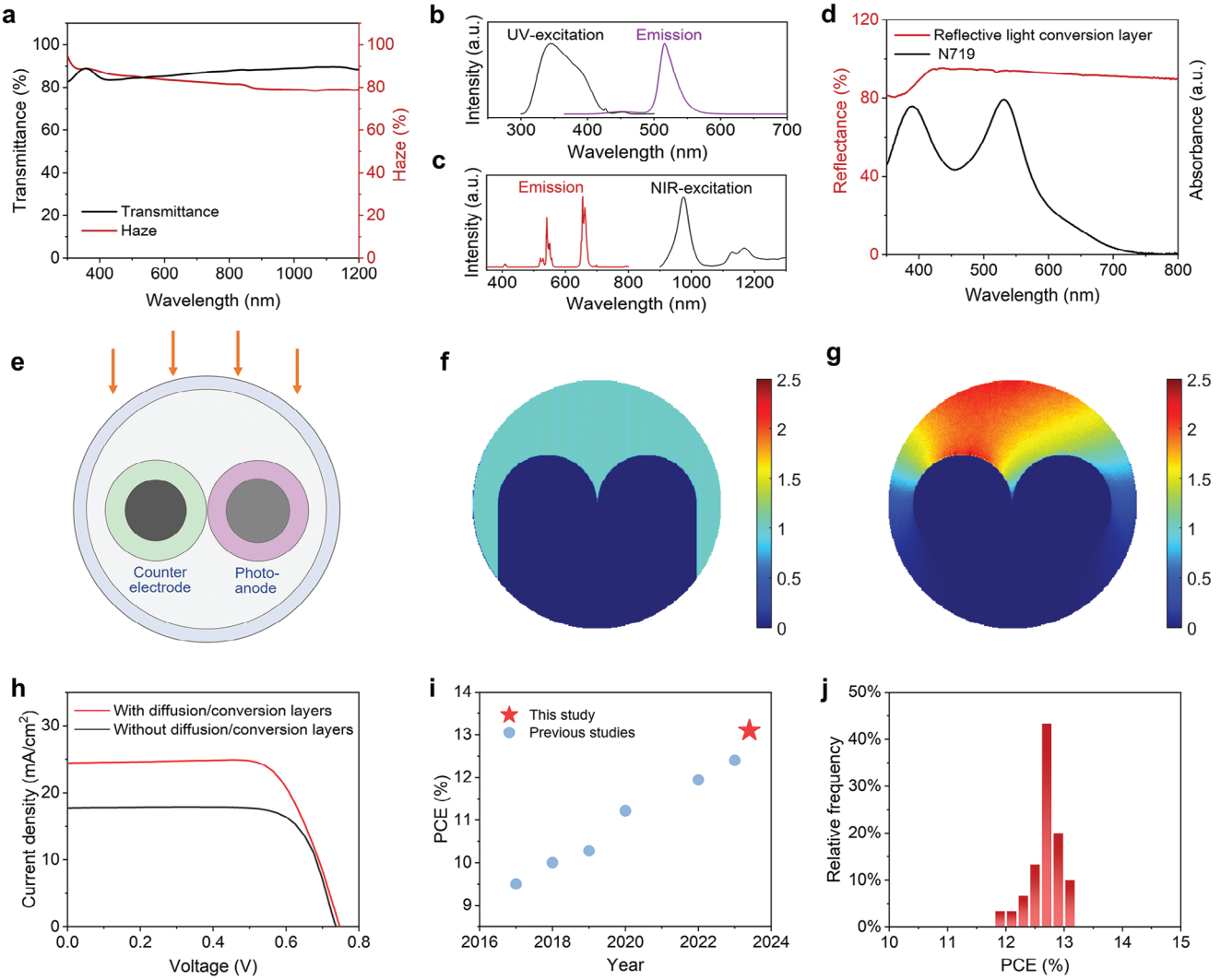

Figure 3. Properties of the designed FDSSC with light diffusion and conversion layers. a) Transmittance and haze spectra of the light diffusion layer. b,c) Fluorescence excitation and emission spectra of the light conversion layer. d) Absorbance spectrum of N719 dye and reflectance spectrum of the light conversion layer. e) Schematic cross-sectional diagram of the designed FDSSC. f,g) Simulated optical field of the incident light in the FDSSC without and with diffusion/conversion layers, respectively. The counter electrode and photoanode are on the left and right, respectively. The incident light experienced strong diffusion and reflection, and optical field neighboring photoanode was reconstructed, effectively improving the utilization of incident light. h) *J–V* curves of FDSSCs with and without diffusion/conversion layers. The PCE of FDSSC without diffusion/conversion layers was 9.84%, with a J_{SC} of 17.730 mA cm^{-2}, a V_{OC} of 0.735 V, and a FF of 0.755. The PCE of FDSSC with diffusion/conversion layers was 13.11%, with a J_{SC} of 24.433 mA cm^{-2}, a V_{OC} of 0.755 V, and a FF of 0.710. i) PCE of the resulting FDSSC in comparison to those of the typical FDSSCs in previous reports. j) PCE statistics of 30 FDSSCs.

With synergistic effects of light diffusion and conversion layers for reconstruction of the inner optical field, the FDSSC efficiently took advantage of the fiber shape to harvest light from various directions and also extended the utilization of solar spectrum, resulting in a significantly enhanced photocurrent (Figure S21, Supporting Information). The FDSSCs barely using UV or NIR excited phosphors both realized high photovoltaic performances with PCEs of 12.76% and 12.92%, respectively (Figure S22, Supporting Information). Finally, the FDSSC with integrated utilization of additional UV and NIR light achieved a record PCE of 13.11%, with J_{SC}, V_{OC}, and FF of 24.433 mA cm^{-2}, 0.755 V, and 0.710, respectively (Figure 3h,i and Figure S23 (Supporting Information)). Owing to the porous structure of light conversion layer that established stable channels for rapid ion diffusions, the resulting FDSSC only exhibited slightly lower FF. By contrast, the dense light conversion layer seriously hindered the migration of ions and caused much higher diffusion impedance, which greatly degenerated the photovoltaic performance of FDSSC, showing a low PCE of 9.43% (Figure S24, Supporting Information).

The PCEs from 30 FDSSCs showed a narrow distribution, demonstrating high repeatability and stable photovoltaic performance of the resulting FDSSCs, which would effectively meet the future demands on large-scale applications (Figure 3j). Moreover, our FDSSCs exhibited high mechanical stabilities with PCE variations below 10% under various deformations of bending, twisting, or pressing for 1000 cycles (Figure S25a, Supporting

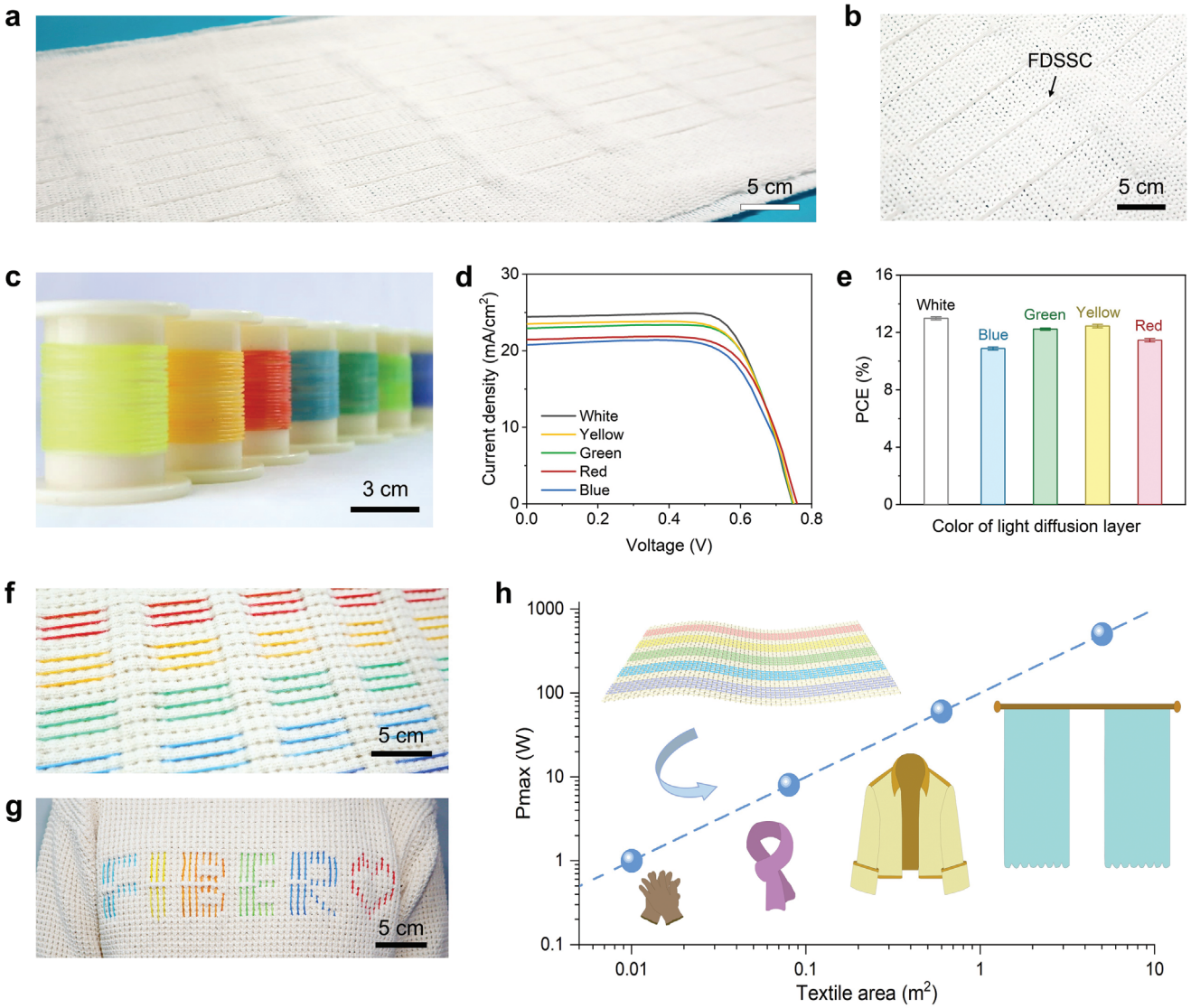

Figure 4. Properties of photovoltaic textiles based on multicolored FDSSCs. a) Photograph of photovoltaic textiles showing a uniform white appearance. b) Magnified photograph of the white photovoltaic textile in (a), in which white FDSSCs were woven together. c) Photograph of FDSSCs with multicolored appearances. d) The corresponding *J*–*V* curves of FDSSCs with light diffusion layers showing different colors. e) PCE values of FDSSCs with light diffusion layers showing different colors. Error bars, standard deviations of the results from five samples. f,g) Photographs of colorful photovoltaic textile composed of color-tunable FDSSCs. h) Theoretically estimated power outputs of various photovoltaic textiles, in which the effective areas accounted for 30%.

Information). These FDSSCs could also operate effectively across a wide temperature range, from −40 to 40 °C, adapting to different environments (Figure S25b, Supporting Information). In addition, after they were placed under outdoor solar exposure in argon condition for 15 days, their performance variations were less than 20% (Figure S26, Supporting Information). And we further explored the PCE dependency of FDSSCs on incident light direction (Figure S27, Supporting Information). The PCEs of FDSSCs had been maintained by over 90% under the incident light from different directions, which is important for practical applications. Moreover, we also measured photovoltaic performances of FDSSCs under outdoor sunlight to investigate their applications in real environments (Figure S28, Supporting Information). The FDSSC without light diffusion and conversion layers exhibited a maximal power density of 7.63 mW cm^{-2} under solar illuminance of 68 500 lx, while the maximum power density of FDSSC with light diffusion and conversion layers was up to 10.39 mW cm^{-2}, showing a remarkable improvement of over 35%.

Inspiringly, the resulting efficient FDSSCs displayed uniform color and appearance, perfectly blended in the textiles, showing high compatibility for wearing applications (**Figure** 4a,b). Meanwhile, we can also introduce colored pigments in light diffusion layer to realize multicolored FDSSCs in addition to the white appearance (Figure 4c and Figure S29 (Supporting Information)), meeting more extensive wearable demands. Owing to the strong light diffusion of Al_2O_3/PU film, few pigments were needed to make FDSSCs display obvious visual colors. The pigments had

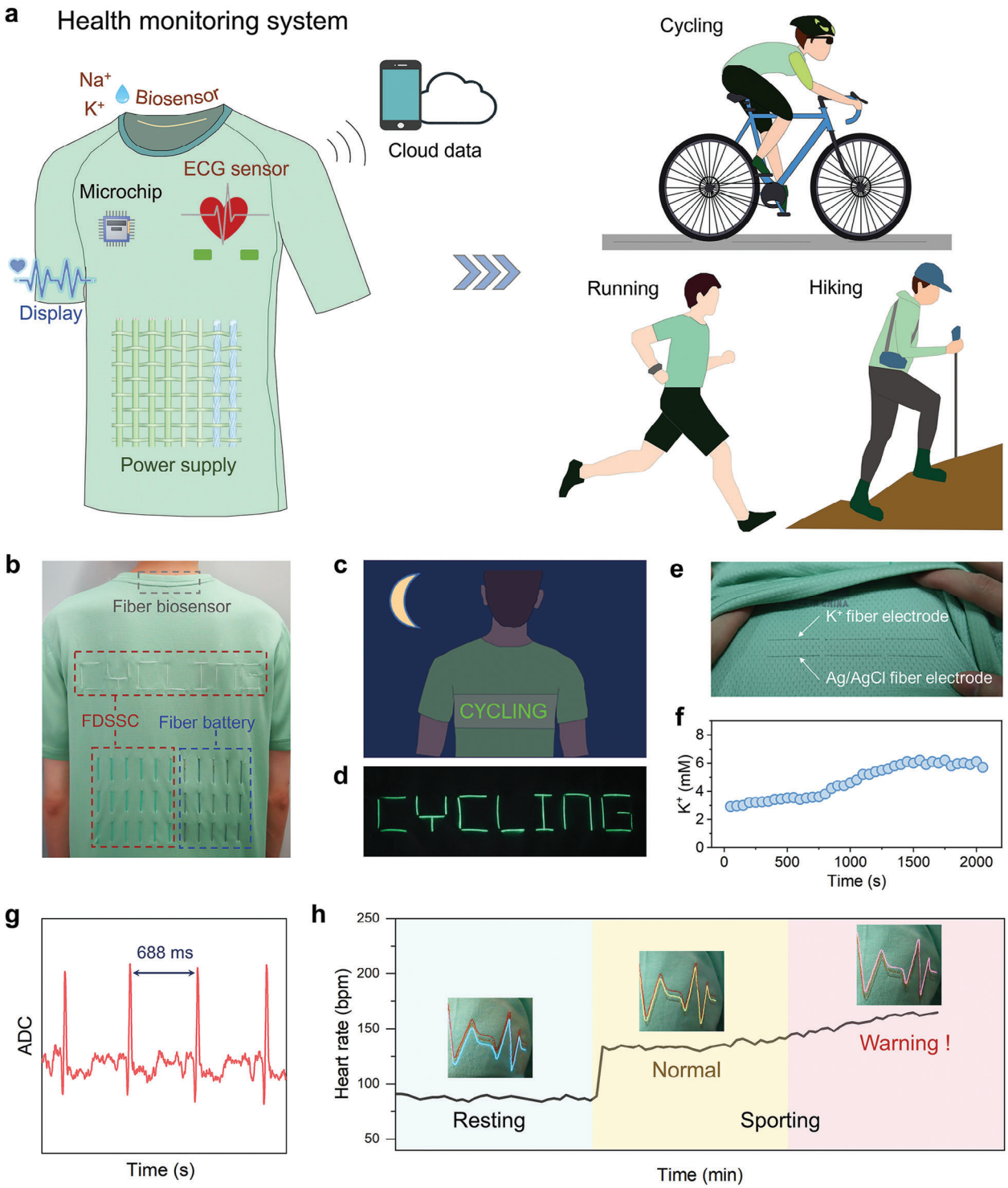

Figure 5. Wearable applications of power supply textiles. a) Schematic showing a smart health monitoring system integrated into daily clothing, including self-charging power supply textile, sensors, and displaying modules, which can collect real-time physiological information from the user at different motion states, and then upload data for analysis and guide a healthy life. b) Photograph of a clothing integrated with color-tunable FDSSCs, fiber batteries, and fiber biosensors. c,d) Diagram and the corresponding photograph of FDSSCs containing luminous powders in the light diffusion layer, which were woven into textiles with designed patterns and could display information at night for warning, respectively. e) Photograph of sweat fiber sensors composed of K^+ working fiber electrodes and Ag/AgCl reference fiber electrode. f) Real-time K^+ concentration in sweat measured by the fiber biosensors. g) Electrocardiogram (ECG) in sweat measured by an ECG sensor. h) Real-time heart rates reflecting physiological status of the user at different motion states, reminding the user with specific displays.

some influence on transmittance at specific visible wavelengths, but the resulting FDSSCs were able to effectively utilize the incident light at NIR wavelengths through light conversion layer, so the colored FDSSCs maintained high photovoltaic performances, e.g., showing high PCEs of 12.45% and 12.13% under yellow and green appearances, respectively (Figure 4d,e and Figure S30 and Table S3 (Supporting Information)). On the contrary, the FDSSCs that used colored package tubes without light diffusion and conversion layers achieved much lower PCEs due to the very limited light harvesting (Figure S31, Supporting Information).

These efficient multicolored FDSSCs can be woven into textiles with multifarious design of sizes and types to meet different power requirements (Figure 4f–h). They were further integrated with fiber batteries as power supply systems, in which the FDSSC modules were connected in series and parallel for the desired output voltages and currents to match the charging voltages and rates of fiber batteries (Figures S32 and S33, Supporting Information). After fiber lithium-ion batteries were charged from 3.0 to 4.4 V by FDSSCs under sunlight, the power supply textile successfully powered a smart bracelet, providing an effective power solution for wearables (Figures S34 and S35, Supporting Information).

Our power supply textiles can also be further integrated with other functional components like sensors, displays, and microchips to construct complex systems, promoting the developments of smart electronic textiles for intelligent life of humans in the future. Here, we illustrated a conceptual health monitoring system integrated into daily clothing (**Figure** 5a and Figures S36 and S37 (Supporting Information)), which was powered by our FDSSCs and fiber batteries (Figure 5b). It can collect real-time physiological information like K^+ ion concentrations and heart rates from the user in different motions by the corresponding sensors (Figure 5e–g). When the user was exercising, the sensors detected relevant physiological information and sent the data to a signal processing chip,[1,25,46] and then the feedback can be reflected in the textile display (Figure S38, Supporting Information). For instance, the data of real-time K^+ concentrations and heart rates collected by the biosensors can be transmitted to mobile phones or laptops, which benefited the user to monitor their health states and make the corresponding diagnoses to evaluate whether it was in a normal range, and if not, the user would be timely alerted with a specific display (Figure 5h). Moreover, besides energy harvesting in the daytime for sustainable power supply, the FDSSCs woven into the textile can also incorporate luminous particles and then display designed patterns at night for warning (Figure 5c,d).

3. Conclusion

In summary, we have designed a FDSSC with a light diffusion layer on the outmost encapsulating tube and a light conversion layer on the inner counter electrode, realizing reconstruction of the optical field in neighboring photoanode. The resulting FDSSC efficiently took advantage of the fiber shape to harvest light from various directions and also extended the utilization of solar spectrum, remarkably enhancing photocurrent to produce a PCE as high as 13.11%. These efficient FDSSCs also realized multicolored appearances, greatly improving their designability and compatibility in real applications. They can be further integrated with fiber batteries into textiles as power systems, which paves the way for supporting the highly desired smart textile systems in the future.

Supporting Information

Supporting Information is available from the Wiley Online Library or from the author.

Acknowledgements

This work was supported by the MOST (Grant Nos. 2022YFA1203001, 2022YFA1203002), the NSFC (Grant Nos. T2321003, 22335003), the STCSM (Grant Nos. 21511104900, 20JC1414902), and the Natural Science Foundation of Jiangsu Province (Grant No. BK20200071).

Conflict of Interest

The authors declare no conflict of interest.

Data Availability Statement

The data that support the findings of this study are available in the supplementary material of this article.

Keywords

dye-sensitized solar cell, fiber, light conversion, light diffusion, smart textile

Received: November 23, 2023
Revised: January 5, 2024
Published online: January 20, 2024

[1] X. Shi, Y. Zuo, P. Zhai, J. Shen, Y. Yang, Z. Gao, M. Liao, J. Wu, J. Wang, X. Xu, Q. Tong, B. Zhang, B. Wang, X. Sun, L. Zhang, Q. Pei, D. Jin, P. Chen, H. Peng, *Nature* **2021**, *591*, 240.
[2] A. Libanori, G. Chen, X. Zhao, Y. Zhou, J. Chen, *Nat. Electron.* **2022**, *5*, 142.
[3] G. Chen, X. Xiao, X. Zhao, T. Tat, M. Bick, J. Chen, *Chem. Rev.* **2022**, *122*, 3259.
[4] M. Dulal, S. Afroj, J. Ahn, Y. Cho, C. Carr, I.-D. Kim, N. Karim, *ACS Nano* **2022**, *16*, 19755.
[5] Y. Sun, Y.-Z. Li, M. Yuan, *Nano Energy* **2023**, *115*, 108715.
[6] Y. Zhang, X. Xia, K. Ma, G. Xia, M. Wu, Y. H. Cheung, H. Yu, B. Zou, X. Zhang, O. K. Farha, J. H. Xin, *Adv. Funct. Mater.* **2023**, *33*, 2301607.
[7] C. Chen, J. Feng, J. Li, Y. Guo, X. Shi, H. Peng, *Chem. Rev.* **2023**, *123*, 613.
[8] Z. Yang, *Pure Appl. Chem.* **2016**, *88*, 113.
[9] M. Hatamvand, E. Kamrani, M. Lira-Cantú, M. Madsen, B. R. Patil, P. Vivo, M. S. Mehmood, A. Numan, I. Ahmed, Y. Zhan, *Nano Energy* **2020**, *71*, 104609.
[10] D. Lv, Q. Jiang, Y. Shang, D. Liu, *npj Flexible Electron.* **2022**, *6*, 38.
[11] Z. Zhu, Z. Lin, W. Zhai, X. Kang, J. Song, C. Lu, H. Jiang, P. Chen, X. Sun, B. Wang, Z. Wang, H. Peng, *Adv. Mater.* **2023**, https://doi.org/10.1002/adma.202304876.

[12] W. Zhai, Z. Zhu, X. Sun, H. Peng, *Adv. Fiber Mater.* **2022**, *4*, 1293.
[13] J. H. Kim, H. W. Park, S. Koo, D. Lee, E. Cho, Y. Kim, M. Shin, J. W. Choi, H. J. Lee, M. Song, *J. Energy Chem.* **2022**, *67*, 458.
[14] M. Batmunkh, T. J. Macdonald, C. J. Shearer, M. Bat-Erdene, Y. Wang, M. J. Biggs, I. P. Parkin, T. Nann, J. G. Shapter, *Adv. Sci.* **2017**, *4*, 1600504.
[15] G. Liu, M. Wang, H. Wang, R. E. A. Ardhi, H. Yu, D. Zou, J. K. Lee, *Nano Energy* **2018**, *49*, 95.
[16] C.-S. Huang, X. Kang, R. M. Rossi, M. V. Kovalenko, X. Sun, H. Peng, L. F. Boesel, *J. Mater. Chem. A* **2021**, *9*, 25974.
[17] R. E. A. Ardhi, M. X. Tran, M. Wang, G. Liu, J. K. Lee, *J. Mater. Chem. A* **2020**, *8*, 2549.
[18] L. Qiu, S. He, J. Yang, F. Jin, J. Deng, H. Sun, X. Cheng, G. Guan, X. Sun, H. Zhao, H. Peng, *J. Mater. Chem. A* **2016**, *4*, 10105.
[19] H. Sun, Y. Zhang, J. Zhang, X. Sun, H. Peng, *Nat. Rev. Mater.* **2017**, *2*, 17023.
[20] X. Xu, S. Xie, Y. Zhang, H. Peng, *Angew. Chem., Int. Ed.* **2019**, *58*, 13643.
[21] J. Zhu, Z. An, A. Zhang, Y. Du, X. Zhou, Y. Geng, G. Chen, *iScience* **2022**, *25*, 104126.
[22] J. Mandal, Y. Fu, A. C. Overvig, M. Jia, K. Sun, N. N. Shi, H. Zhou, X. Xiao, N. Yu, Y. Yang, *Science* **2018**, *362*, 315.
[23] X. Meng, C. Yu, X. Zhang, L. Huang, M. Rager, J. Hong, J. Qiu, Z. Lin, *Nano Energy* **2018**, *54*, 138.
[24] L. Yao, Q. Wu, P. Zhang, J. Zhang, D. Wang, Y. Li, X. Ren, H. Mi, L. Deng, Z. Zheng, *Adv. Mater.* **2018**, *30*, 1706054.
[25] J. He, C. Lu, H. Jiang, F. Han, X. Shi, J. Wu, L. Wang, T. Chen, J. Wang, Y. Zhang, H. Yang, G. Zhang, X. Sun, B. Wang, P. Chen, Y. Wang, Y. Xia, H. Peng, *Nature* **2021**, *597*, 57.
[26] Z. Zhu, Z. Lin, Y. Gu, J. Song, X. Kang, H. Jiang, H. Peng, *Adv. Funct. Mater.* **2023**, *33*, 2306742.
[27] J. Peoples, X. Li, Y. Lv, J. Qiu, Z. Huang, X. Ruan, *Int. J. Heat Mass Transfer* **2019**, *131*, 487.
[28] Y. Liang, B. Qiao, T. Wang, H. Gao, K. Yu, *Appl. Surf. Sci.* **2016**, *387*, 581.
[29] Z. Ge, Y. Luo, *Prog. Org. Coat.* **2013**, *76*, 1522.
[30] S. Wang, P. Chen, J. Yeh, K. Chen, *React. Funct. Polym.* **2007**, *67*, 299.
[31] B. K. Kim, J. C. Lee, *J. Polym. Sci., Part A: Polym. Chem.* **1996**, *34*, 1095.
[32] A. Miffre, D. Cholleton, P. Rairoux, *Opt. Lett.* **2020**, *45*, 1084.
[33] A. Bhardwaj, N. M. Puthoor, G. G. Nair, *J. Phys. Chem. C* **2020**, *124*, 18698.
[34] S. Hříbalová, P. Šimonová, W. Pabst, *J. Eur. Ceram. Soc.* **2024**, *44*, 1163.
[35] F. Lin, B. Xue, H. Huang, L. Zhu, S. Yang, *Carbohydr. Polym.* **2022**, *294*, 119804.
[36] T. Naganuma, Y. Kagawa, *J. Mater. Sci.* **2003**, *38*, 3103.
[37] A. Dorodnyy, J. Smajic, J. Leuthold, *Laser Photonics Rev.* **2023**, *17*, 2300055.
[38] X. Ouyang, P. Li, D. Chen, J. Tang, *J. Appl. Polym. Sci.* **2016**, *133*, 42923.
[39] E. Klampaftis, D. Ross, K. R. McIntosh, B. S. Richards, *Sol. Energy Mater. Sol. Cells* **2009**, *93*, 1182.
[40] B. C. Rowan, L. R. Wilson, B. S. Richards, *IEEE J. Sel. Top. Quantum Electron.* **2008**, *14*, 1312.
[41] N. Yao, J. Huang, K. Fu, X. Deng, M. Ding, X. Xu, *RSC Adv.* **2016**, *6*, 17546.
[42] T. Chen, Y. Shang, S. Hao, L. Tian, Y. Hou, C. Yang, *Electrochim. Acta* **2018**, *282*, 743.
[43] A. Budo, I. Ketskemety, *J. Chem. Phys.* **1956**, *25*, 595.
[44] W. Bae, T.-Y. Yoon, C. Jeong, *PLoS One* **2021**, *16*, e0247326.
[45] S. L. Jacques, L. Wang, in *Optical-Thermal Response of Laser-Irradiated Tissue* (Eds: A. J. Welch, M. J. C. Van Gemert), Springer, Boston, MA **1995**.
[46] L. Wang, L. Wang, Y. Zhang, J. Pan, S. Li, X. Sun, B. Zhang, H. Peng, *Adv. Funct. Mater.* **2018**, *28*, 1804456.